Available online at www.sciencedirect.com
SCIENCE DIRECT
Image and Vision Computing 23 (2005) 1192–1202
image AND vision COMPUTING
www.elsevier.com/locate/imavis

Lane following and lane departure using a linear-parabolic model

Cláudio Rosito Jung*, Christian Roberto Kelber

UNISINOS-Universidade do Vale do Rio dos Sinos, PIPCA-Graduate School of Applied Computing, Av. UNISINOS, 950, 93022-000 São Leopoldo, RS, Brasil

Received 21 September 2004; received in revised form 18 July 2005; accepted 26 July 2005

Abstract

This paper proposes a technique for unwanted lane departure detection. Initially, lane boundaries are detected using a combination of the edge distribution function and a modified Hough transform. In the tracking stage, a linear-parabolic lane model is used: in the near vision field, a linear model is used to obtain robust information about lane orientation; in the far field, a quadratic function is used, so that curved parts of the road can be efficiently tracked. For lane departure detection, orientations of both lane boundaries are used to compute a lane departure measure at each frame, and an alarm is triggered when such measure exceeds a threshold. Experimental results indicate that the proposed system can fit lane boundaries in the presence of several image artifacts, such as sparse shadows, lighting changes and bad conditions of road painting, being able to detect in advance involuntary lane crossings.

Keywords: Machine vision; Hough transform; Lane detection; Lane following; Lane departure; Driver assistance system

1. Introduction

Nowadays, an important social and economic problem regards traffic safety. According to the United Nations [1], 1.26 million people died globally in road related accidents in 2000, leading to an average toll of 3000 fatalities a day. In particular, road-related accidents are a major concern in developing countries. The annual report of the Brazilian national traffic department (DENATRAN) of 2002 [2] shows a total of 250,000 accidents, with around 20,000 fatalities only in Brazil (unofficial statistics point to over 50,000 traffic-related deaths in Brazil in 2004). A considerable fraction of this total is due to driver fatigue and/or inattention. In many cases, the driver falls asleep (mostly bus and truck drivers), making the vehicle to leave its designated lane and possibly causing and accident.

It is expected that machine vision systems can be used to improve safety on the roads, decreasing the number of accidents. Particularly, an efficient lane departure warning system could alert the driver and possibly prevent an accident. In fact, several researchers worldwide have been developing vision-based systems for lane detection, lane following and lane departure warning. However, most of them present limitations in situations involving shadows, varying illumination conditions, bad conditions of road paintings and other image artifacts. Next, some of these techniques are briefly described.

One class of lane detection methods [3,4] relies on top-view (birds eye) images computed from images acquired by the camera. These methods are reliable in obtaining lane orientation in world coordinates, but require online computation of the top-view images (and camera calibration).

Deformable road models have been widely used for lane detection and tracking [5–9]. Such techniques rely on mathematical models to fit road boundaries. In general, simpler models (e.g. linear) do not provide an accurate fit, but they are more robust with respect to image artifacts. On the other hand, more complex models (such as parabolic and splines) are more flexible, but also more sensitive to image artifacts/noise.

Apostoloff and Zelinsky [10] proposed a lane tracking system based on particle filtering and multiple cues. In fact, this method does not track explicitly the lanes, but it computes parameters such as lateral offset and yaw of the vehicle with respect to the center of the road. Although the method appears to be robust under a variety of conditions

* Corresponding author. Tel.: +55 51 591 1122x1626; fax: +55 51 590 8172.
E-mail addresses: crjung@unisinos.br (C.R. Jung), kelber@unisinos.br (C.R. Kelber).

0262-8856/$ - see front matter © 2005 Elsevier Ltd All rights reserved.
doi:10.1016/j.imavis.2005.07.018

(shadows, different lighting conditions, etc.), it cannot be used to estimate curvature or detect if the vehicle is approaching a curved part of the road.

McCall and Trivedi [11] proposed a method for lane detection using steerable filters. Such filters perform well in picking out both circular reflector road markings as well as painted line road markings. Filter results are then processed to eliminate outliers based on the expected road geometry and used to update a road and vehicular model along with data taken internally from the vehicle. Such technique is robust with respect to lighting changes and shadows, but has shortcomings for relatively curved roads (because this method relies basically on a linear model).

LeBlanc et al. [12] proposed a road-departure prevention system, that predicts the vehicles's path and compares such path with the sensed road geometry to estimate the time to lane-crossing (TLC). However, the vision-based sensor requires good lighting and pavement conditions to detect lane boundaries.

Risack et al. [13] proposed a lane keeping assistance system, which warns the driver on unintended lane departures. In fact, they used an existing videobased lane detection algorithm and compared different methods to detect lane departure, using several assumptions on driver behavior in certain situations to distinguish between intended and unintended lane departures. Lane departures are successfully detected, by their technique, but they also needed roads in good conditions and lighting conditions.

Lee [14] proposed a lane departure detection system that estimates lane orientation through an edge distribution function (EDF), and identifies changes in the travelling direction of a vehicle. However, the EDF may fail in curved roads with dashed lane markings. A modification of this technique [15] includes a boundary pixel extractor to improve its robustness. However, curved lanes may still cause problems, because a linear model (computed using the Hough transform) is used for fitting lane boundaries.

This paper focuses on non-ideal road conditions (weak lane markings), which are common in developing countries such as Brazil. We use a linear-parabolic model [16] for lane boundaries, that consists of a linear function in the near field (locally, the road is assumed to be straight), and a quadratic function in the far field (such that incoming curves can be efficiently detected). This model combines the robustness of the linear model with the flexibility of the parabolic model, showing good detection results in the presence of noise, sparse shadows, different illumination conditions and weak lane markings. The orientation of both lane boundaries in the near field is used to provide a measure of deviation from the center of the lane.

The remainder of this paper is organized as follows. Our approach for initial lane detection is described in Section 2, and the lane following approach based on a linear-parabolic lane model is presented in Section 3. Our lane departure warning system is described in Section 4. Section 5 illustrates some experimental results, and concluding remarks are presented in Section 6.

2. Initial lane detection

In this stage, the first frame acquired by the camera is processed, and the two (left and right) lane boundaries are obtained automatically. Our coordinate system coincides with image coordinates, and a threshold x_m separates the near and far vision fields, as shown in Fig. 1. The choice for x_m depends on the size the acquired images and the tilt angle of the camera, and should result in a length of about 10 m for the near field (in a typical camera installation with resolution of 240×320 pixels, it is possible to see about 30–40 m ahead with reasonable definition).

For the initial detection, we chose a linear model for the lane boundary, because of its simplicity and robustness. We also assume that the following conditions are satisfied in the first frame of the video sequence:

- the vehicle is initially located in a straight portion of the road;
- the vehicle is approximately aligned with the road;
- there are no significant linear structures in the image, except for the lane boundaries.

To detect the linear lane boundaries, we combine the EDF approach adopted by Lee [14] with the Hough transform [17].

2.1. The edge distribution function

For the greyscale image $I(x,y)$, the gradient function $\nabla I(x,y)$ can be approximated by:

$$\nabla I(x,y) = \left(\frac{\partial I}{\partial x}, \frac{\partial I}{\partial y}\right)^T \approx (D_x, D_y)^T, \quad (1)$$

where D_x and D_y are differences computed in the x and y directions (this differences can be computed using the Sobel operator [18]). We can estimate the gradient magnitude and orientation using the following equations:

$$|\nabla I(x,y)| \approx |D_x| + |D_y|, \quad (2)$$

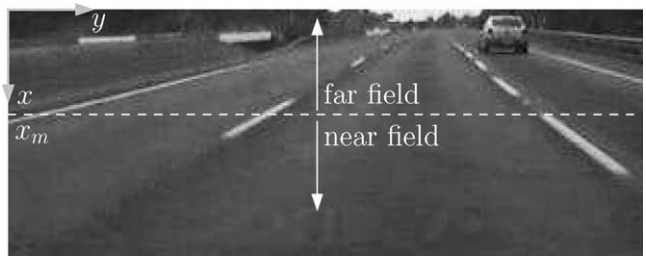

Fig. 1. Our coordinate system and the definition of the near and far fields.

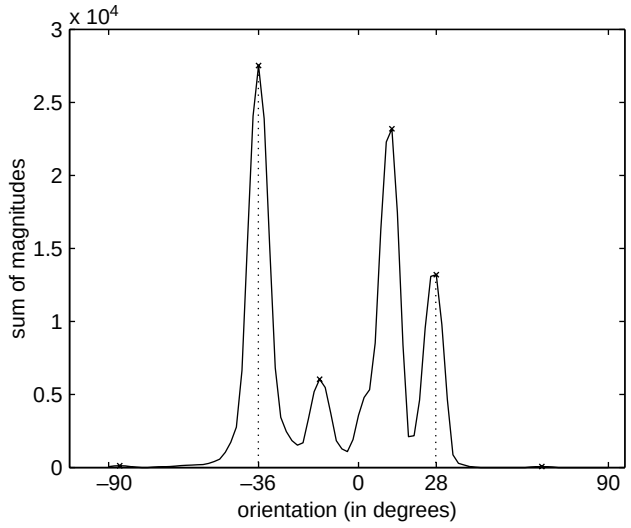

Fig. 2. Smoothed edge distribution function (EDF).

$$\theta(x,y) = \frac{1}{2}\tan^{-1}\left(\frac{\sum_{(u,v)\in R} 2D_x(u,v)D_y(u,v)}{\sum_{(u,v)\in R}(D_x(u,v)^2 - D_y(u,v)^2)}\right), \quad (3)$$

where R is a $(2L+1)\times(2L+1)$ region centered at pixel (x, y). Eq. (3) represents the least squares angular estimation within R [19], and produces better results than simply computing $\tan^{-1}(D_y/D_x)$. We used $L=1$ in this work, so that a small 3×3 neighborhood is used for angle estimation.

To determine the orientation of the road boundaries, we compute the edge distribution function (EDF), which is the histogram of the gradient magnitude with respect to the orientation[1]. To compute this histogram, the angles $\theta(x, y)$ within the range $[-90, 90°]$ were quantized in 90 subintervals (each one with length of 2°). A lookup table can be used to avoid the computation of $\tan^{-1}$ in Eq. (3).

Considering that lanes are the only significant linear objects in the image, and that the car is aligned with the central axis of the road, it is expected that lanes boundaries will generate two local maxima in the EDF. However, multi-lane roads generate several local maxima. In fact, Fig. 1 illustrates a road with three travelling lanes (and the vehicle is located in the middle lane). Fig. 2 illustrates the EDF (a Gaussian filter was used to smooth the histogram) for this image, and four local maxima can be observed. The first one (at $\theta=-36°$) is related to the right boundary of the central lane; the second one (at $\theta=-14°$) is related to the right boundary of the right lane; the third one (at $\theta=12°$) is related to the left boundary of the left lane; finally, the last one (at $\theta=28°$) is related to the left boundary of the central lane.

In general, inner lane boundaries (where the car is travelling) have approximately symmetric orientations and are closer to vertical lines in the image (i.e. correspond to smallest and largest values of θ in the EDF). If α_1 and α_2 denote the smallest and largest orientations of the EDF, respectively, then they are kept if:

$$|\alpha_1 + \alpha_2| < T_1, \quad (4)$$

where T_1 is a threshold ($T_1=15°$ was used in all experiments). In Fig. 2, it can be noticed that $\alpha_1=-36°$ and $\alpha_2=28°$ satisfy such conditions, and are retrieved.

Lee [14] used the EDF to determine the orientation of each lane boundary. However, we want to detect these boundaries explicitly, by fitting a linear function. Let α be the orientation corresponding to the desired lane boundary. Also, let $g(x, y)$ be the directional edge image defined as:

$$g(x,y) = \begin{cases} |\nabla I(x,y)|, & \text{if } |\theta(x,y)-\alpha| < T_2 \\ 0, & \text{otherwise} \end{cases}, \quad (5)$$

where T_2 is an angular threshold (in this work, we used $T_2=2°$, to match the quantization used in computation of the EDF). It should be noticed that $g(x, y)$ contains edge magnitudes of the original image $I(x, y)$ that are aligned with the direction α. These magnitudes will be mostly related to the lane boundary, but some pixels related to noise or other structures that are aligned with the lane may also appear. Fig. 3 shows image $g(x, y)$ for $\alpha=-36°$, which corresponds to the right lane boundary. Indeed, some isolated pixels with small magnitude that are not related to this lane boundary appear in the image.

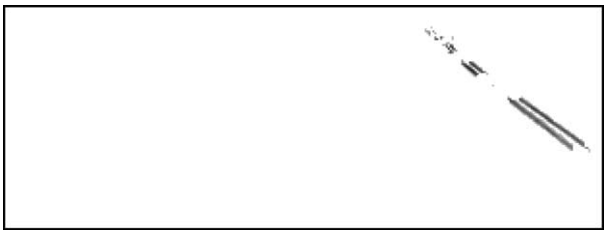

Fig. 3. Magnitudes aligned with the right lane boundary.

2.2. The Hough transform

Applying the Hough transform to a set of edge points (x_i, y_i) results in an 2D function $C(\rho, \theta)$ that represents the number of edge points satisfying the linear equation $\rho=x\cos\theta+y\sin\theta$. In practical applications, the angles θ and distances ρ are quantized, and we obtain an array $C(\rho_k, \theta_l)$. The local maxima of $C(\rho_k, \theta_l)$ can be used to detect straight line segments passing through edge points.

In our case, the orientation θ can be obtained from the EDF peak α described in Section 2.1 (in fact, we have $\theta=\alpha$, as shown in Fig. 4). Thus, we have a one-dimensional search (only the parameter ρ_k). Also, instead of building $C(\rho_k, \alpha)$ by counting the number of edge pixels belonging to $\rho_k=x\cos\alpha+y\sin\alpha$, we use an alternative approach, based on the gradient weighted Hough transform [20].

[1] Please, note that the gradient direction is orthogonal to the contour orientation.

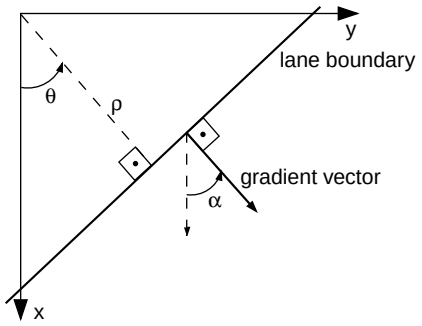

Fig. 4. Relation between the EDF peak α and the parameters ρ and θ of the Hough transform.

Let (x_i, y_i), for $i=1,\ldots,n$, be the coordinates of non-zero pixels of the threshold magnitude image $g(x, y)$ corresponding to the orientation α. We define $C(\rho_k, \alpha)$ as:

$$C(\rho_k, \alpha) = \sum_j g(x_j, y_j), \tag{6}$$

where (x_j, y_j) are all the edge pixels belonging to $\rho_k = x \cos \alpha + y \sin \alpha$. By summing edge magnitudes instead of counting the number of aligned pixels, we minimize the influence of edges with small magnitudes (typically related to noise). If ρ_α denotes the global maximum of $C(\rho_k, \alpha)$, the lane boundary corresponding to the EDF peak α is given by the straight line:

$$y = -x \cot \alpha + \frac{\rho_\alpha}{\sin \alpha}. \tag{7}$$

This line detection procedure is applied independently to each lane boundary, resulting in one linear model for each boundary. This initial detection is used to find the lane boundary region of interest (LBROI), which will be the search space for lane boundaries in the subsequent frame of the video sequence. In this work, the LBROI is obtained by 'thickening' the detected lane boundary, such that it is extended $w(x)$ pixels to the right and $w(x)$ pixels to the left in the y direction. Due to camera perspective, LBROIs should be thinner at the top of the image (far field), and fatter at the bottom (near field). A simple choice for $w(x)$ is a linear function, stretching w_{bottom} pixels to both sides at the bottom and w_{top} pixels at the top. The LBROIs shown in Fig. 5 correspond to the lane boundaries depicted in Fig. 1, using $w_{\text{bottom}} = 12$ and $w_{\text{top}} = 6$ pixels.

Fig. 5. LBROIs corresponding to the initial lane segmentation using the linear model.

3. Lane following

After the initial segmentation in the first frame, we need to update the detection for subsequent frames. For the initial detection, a linear model was chosen, because it provides a robust automatic detection. However, this model is obviously not suitable for curved roads. In this paper, we propose a lane boundary model that is flexible enough to follow curved roads, robust with respect to road/background variations (noise, sparse shadows, weak lane markings), and that can provide information about lane orientation and/or curvature. This model is described next.

3.1. The proposed lane boundary model

Let us consider the following model $f(x)$ for lane boundary:

$$f(x) = \begin{cases} a + bx, & \text{if } x > x_m \\ c + dx + ex^2, & \text{if } x \le x_m \end{cases}, \tag{8}$$

where x_m represents the border between near and far fields, as shown in Fig. 1. If we impose continuity and differentiability conditions on the function f, we must have $f(x_m^+) = f(x_m^-)$ and $f'(x_m^+) = f'(x_m^-)$. These conditions imply that:

$$\begin{cases} a + bx_m = c + dx_m + ex_m^2 \\ b = d + 2ex_m \end{cases}. \tag{9}$$

Solving this system for variables c and e, and replacing the result back into Eq. (9) leads to:

$$f(x) = \begin{cases} a + bx, & \text{if } x > x_m \\ \dfrac{2a + x_m(b-d)}{2} + dx + \dfrac{(b-d)}{2x_m}x^2, & \text{if } x \le x_m \end{cases}. \tag{10}$$

Eq. (10) indicates that our lane boundary model is characterized by only three coefficients (a, b and d). To determine these parameters, we use a weighted least squares method, fitting the proposed model to the images acquired by the camera. This procedure is applied independently for each lane boundary, and is described next.

3.2. Fitting the linear-parabolic model

Let us assume that both (right and left) lane boundaries were detected in the prior frame of the video sequence. In the current frame, it is expected that lane boundaries will be constrained to a neighborhood of the prior detection (this region is the LBROI, as defined in the prior Section).

The edge image $|\nabla I(x,y)|$ of the current frame is computed within the LBROI. Although most of the edges will be related to the lane boundary, some edges related to noise, road texture or other structures would also appear.

To remove these undesired edges, we apply an adaptive threshold based on the mean magnitude M_{mean} of the edges. More specifically, we remove all the edges with magnitudes smaller than 0.5 M_{mean}. Let $g(x,y)$ denote the thresholded edge image:

$$g(x,y) = \begin{cases} |\nabla I(x,y)|, & \text{if } |\nabla I(x,y)| \geq 0.5 M_{\text{mean}} \\ 0, & \text{otherwise} \end{cases}. \quad (11)$$

It should be noticed that this adaptive threshold is not affected by varying illumination conditions, and does not require any a priori information about color and/or contrast between the road and lane markings. For example, Fig. 6 shows the thresholded edge image $g(x, y)$ for the frame subsequent to the one illustrated in Fig. 5.

Let (x_{n_i}, y_{n_i}), for $i=1, \ldots, m$, denote the m coordinates of the non-zero pixels of the thresholded edge image $g(x,y)$ belonging to the near field, and $M_{n_i} = g(x_{n_i}, y_{n_i})$ the respective magnitudes. Analogously, let (x_{f_j}, y_{f_j}) and $M_{f_j} = g(x_{f_j}, y_{f_j})$, for $j=1, \ldots, n$, represent the same characteristics for the n edge pixels in the far field.

Fitting the lane model (10) to the edge data results in a linear system with three unknowns and $n+m$ equations:

$$\begin{cases} a + b x_{n_i} = y_{n_i}, & \text{for } i = 1, 2, \ldots, m \\ \dfrac{2a + x_m(b-d)}{2} + d x_{f_j} & \\ \quad + \dfrac{(b-d)}{2x_m} x_{f_j}^2 = y_{f_j}, & \text{for } j = 1, 2, \ldots, n \end{cases}. \quad (12)$$

Typically, $(n+m)$ will be much greater than three, and this system will not admit an exact solution. However, we can find an approximated solution such that a specific error measure is minimized. Assuming that edges related to lane boundaries usually have larger magnitudes than edges related to other irrelevant structures (such as noise, road texture, etc.), we propose a quadratic error weighted by the respective edge magnitudes:

$$E = \sum_{i=1}^{m} M_{n_i} [y_{n_i} - f(x_{n_i})]^2 + \sum_{j=1}^{n} M_{f_j} [y_{f_j} - f(x_{f_j})]^2. \quad (13)$$

Such error E can be written as:

$$E = (\mathbf{b} - \mathbf{Ac})^{\mathrm{T}} \mathbf{W} (\mathbf{b} - \mathbf{Ac}), \quad (14)$$

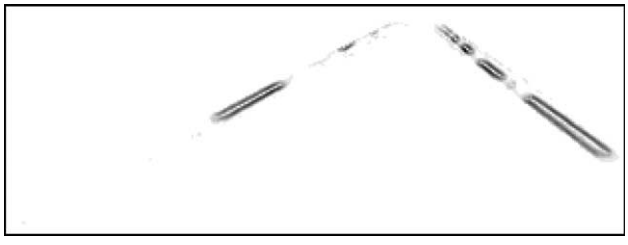

Fig. 6. Thresholded edge image corresponding to the LBROIs depicted in Fig. 5 for the subsequent frame (darker pixels relate to larger magnitudes).

and is minimized when the following 3×3 linear system is solved:

$$\mathbf{A}^{\mathrm{T}} \mathbf{WAc} = \mathbf{A}^{\mathrm{T}} \mathbf{Wb}, \quad (15)$$

where:

$$\mathbf{A} = \begin{bmatrix} 1 & x_{n_1} & 0 \\ \vdots & \vdots & \vdots \\ 1 & x_{n_m} & 0 \\ 1 & \dfrac{1}{2x_m}(x_{f_1}^2 + x_m^2) & -\dfrac{1}{2x_m}(x_{f_1} - x_m)^2 \\ \vdots & \vdots & \vdots \\ 1 & \dfrac{1}{2x_m}(x_{f_n}^2 + x_m^2) & -\dfrac{1}{2x_m}(x_{f_n} - x_m)^2 \end{bmatrix},$$

$$\mathbf{W} = \mathrm{diag}(M_{n_1}, \ldots, M_{n_m}, M_{f_1}, \ldots, M_{f_n}),$$

$$\mathbf{c} = [a, b, d]^T \text{ and } \mathbf{b} = [y_{n_1}, \ldots, y_{n_m}, y_{f_1}, \ldots, y_{f_n}]^{\mathrm{T}}.$$

Fig. 7 shows the lane boundaries detected by fitting the proposed model to the edge magnitudes illustrated in Fig. 6. Due to the minimization process, the model is fitted at the center of lane markings (thus, we do not have to deal with inner and outer boundaries, as done in [15]). Also, it should be noticed that a straight portion of the road is depicted. Consequently, the parabolic part of our model is approximately linear.

An LBROI is associated to each lane boundary, using the same procedure applied in the initial segmentation. In the subsequent frame, the edge image will be computed only in a small region delimited by the LBROI obtained in the current frame. The procedure described in Section 3.2 is then repeated for the remaining frames. Our lane following algorithm performs well even in roads having weak lane markings, as long as there is enough edge information about lane boundaries. An example of fitting the model to a poorly marked road is shown in Fig. 8. The original image is shown in Fig. 8(a), and it contains small and worn-off lane markings. However, there is enough edge information about lane boundaries in the LBROI, as illustrated in Fig. 8(b). The result of fitting the linear-parabolic model is depicted in Fig. 8(c). Due to camera perspective, edge information is

Fig. 7. Detected lane boundaries.

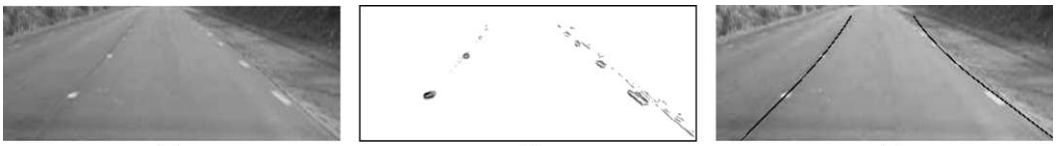

Fig. 8. (a) Image with weak lane markings. (b) Thresholded edge magnitudes within LBROIs. (c) Detected lane boundaries.

weaker in the far field, which tends to produce some oscillation in the parabolic part of the model when lane markings are very poor.

The proposed lane following algorithm is very efficient in terms of computational requirements. Initially, the edge image is computed only within the two LBROIs, which contain approximately $h\times(w_{\text{bottom}}+w_{\text{top}})$ pixels, where h is the height of the original image. After thresholding the edge image with respect to the mean gradient magnitude, about 35% of these pixels are removed. Them to solve Eq. (15), we need to compute matrix products $\mathbf{A}^{\mathrm{T}}\mathbf{WA}$ and $\mathbf{A}^{\mathrm{T}}\mathbf{Wb}$ for each lane boundary, where $\mathbf{A}$ is a $(n+m)\times 3$ matrix, $\mathbf{W}$ is a diagonal matrix, b is a $1\times(n+m)$ vector, and $n+m$ is the number of edge pixels remaining after thresholding. Approximately $18(n+m)$ multiplications are involved in such computations (it should be noticed that only the lower triangular portion of $\mathbf{A}^{\mathrm{T}}\mathbf{WA}$ must be computed, since it is a symmetric matrix). Computational time to solve the 3×3 system described in Eq. (15) is neglectable. Typically, we use 240×320 images, with $w_{\text{bottom}}=12$ and $w_{\text{top}}=6$, resulting in $n+m\approx 756$ for each lane boundary after the thresholding process. Although execution time depends on edge information, an implementation of the proposed technique in C++ can usually process up to 100 FPS running in a portable computer powered by a Pentium Centrino 1.7 GHz with 1 GB RAM memory.

4. Lane departure detection

If the vehicle is travelling in a straight portion of the road and stays at the center of the lane, we should expect symmetry (for the near vision field) in the orientations of left and right lane boundaries ($\theta_{\mathrm{l}}+\theta_{\mathrm{r}}=0$), as depicted in Fig. 9. If the vehicle drifts to its left, both θ_{l} and θ_{r} increase. If the vehicle drifts to its right, both θ_{l} and θ_{r} decrease. In any case, the value $|\theta_{\mathrm{l}}+\theta_{\mathrm{r}}|$ gets away from zero. Thus, a simple and efficient measure for trajectory deviation is given by:

$$\beta = |\theta_{\mathrm{l}} + \theta_{\mathrm{r}}|. \tag{16}$$

If β gets sufficiently large, the vehicle is leaving the center of the lane. In this work, β is compared to a threshold T_3, and a lane departure warning is issued if $\beta > T_3$. Experimental results indicate that $T_3=15°$ is a good choice, coinciding with threshold T_1 used in the initial lane detection algorithm).

In the previous Section, we have derived explicit models for left and right lane boundaries, that are denoted by $f_l(x)$ and $f_r(x)$, respectively. Such models can be used to determine orientations $\theta_l\,(x)$ and $\theta_r(x)$:

$$\theta_{\mathrm{l}}(x) = \tan^{-1}(f_{\mathrm{l}}'(x)), \qquad \theta_{\mathrm{r}}(x) = \tan^{-1}(f_{\mathrm{r}}^{1}(x)). \tag{17}$$

Eq. (17) provides orientations $\theta_{\mathrm{l}}\,(x)$ and $\theta_{\mathrm{r}}(x)$ at any position x. However, to compute the symmetry measure β, we need to determine such orientations in the near field (to obtain the vehicle's current orientation). In fact, $\theta_{\mathrm{l}}\,(x)=\theta_{\mathrm{l}}$ and $\theta_{\mathrm{r}}(x)=\theta_{\mathrm{r}}$ are actually constant values within the near field, because $f_{\mathrm{l}}(x)$ and $f_{\mathrm{r}}(x)$ are both linear functions for any $x\geq x_m$.

To reduce the influence of noise, temporal filtering is applied to estimate θ_{l} and θ_{r}, by averaging orientations in consecutive frames. If θ_{l}^{k} and θ_{r}^{k} denote orientations in the kth frame of the video sequence, then orientations in the current frame n are given by:

$$\theta_{\mathrm{l}}^{n} = \sum_{k=0}^{4} \theta_{\mathrm{l}}^{n-k} \text{ and } \theta_{\mathrm{r}}^{n} = \sum_{k=0}^{4} \theta_{\mathrm{r}}^{n-k} \tag{18}$$

In general, lane departures can be classified as wanted or unwanted. In the first case, the driver makes a voluntary lane change (to overtake a car, for example), and turns on the blinker to indicate his intent. The second case corresponds to involuntary lane changes that usually occur when the driver falls asleep or is not paying attention to the road. These cases are treated differently by our algorithm.

For involuntary lane changes, the system triggers an alarm whenever $\beta > T_3$ (such that driver can correct his trajectory as soon as possible). However, for voluntary changes (that are detected if the blinker is on), the system does not trigger any alarm. Instead, it waits until lane shift is completed, and recomputes lane boundaries. If the vehicle changes to its left lane, the former left lane boundary will become the new right lane boundary, and the new left lane boundary will be computed using the initial lane detection algorithm described in Section 2. For shifts to the right lane, an analogous procedure is applied.

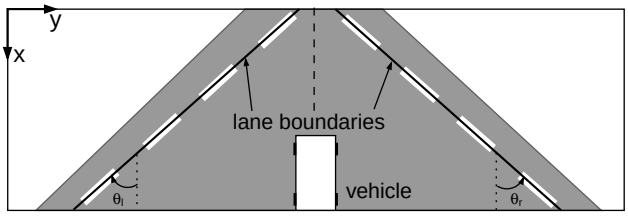

Fig. 9. Orientation of lane boundaries.

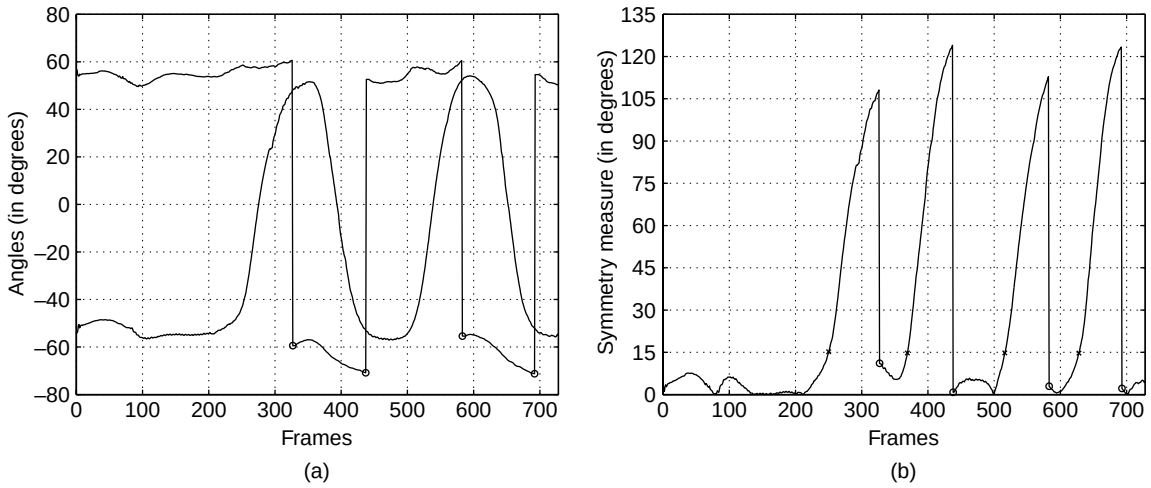

Fig. 10. (a) Orientations θ_r and θ_l for the first video sequence. (b) Corresponding symmetry measure α.

5. Experimental results

We tested the proposed technique for several video sequences containing varying illuminations conditions, shadows and poor lane painting. All sequences were captured with a resolution of 240×320 pixels, at 15 FPS.

The first video sequence contains 728 frames, and illustrates four lane changes. Orientations θ_l and θ_r are shown in Fig. 10(a), and the symmetry measure β is illustrated in Fig. 10(b). Such data indicates that the vehicle shifts to the left lane, and right after returns to its original lane (this movement is related to overtaking a motorcycle). Some time later, the vehicle repeats these successive lane changes again (the driver was simulating an overtake). Since the blinker was activated in all lanes shifts, no lane departure warnings were issued. Some frames of this sequence are shown in Fig. 11. In particular, we notice that the vehicle is just beginning to change lanes at frames 250 and 516 (when lane departure was detected), and driver could have been alerted on time to avoid an accident in case of unwanted lane departure. It is also interesting to notice that lane boundaries were correctly adjusted even in the presence of intense shadow contamination (frames 315–390).

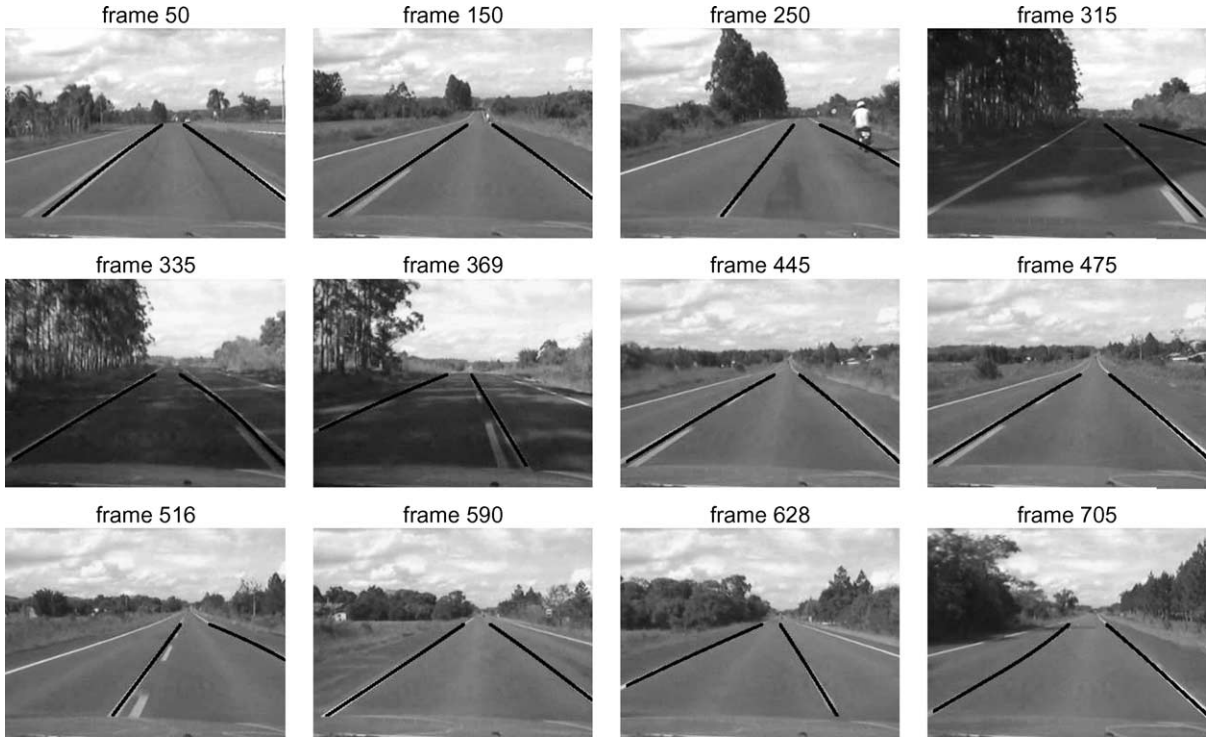

Fig. 11. Twelve frames from the first video sequence.

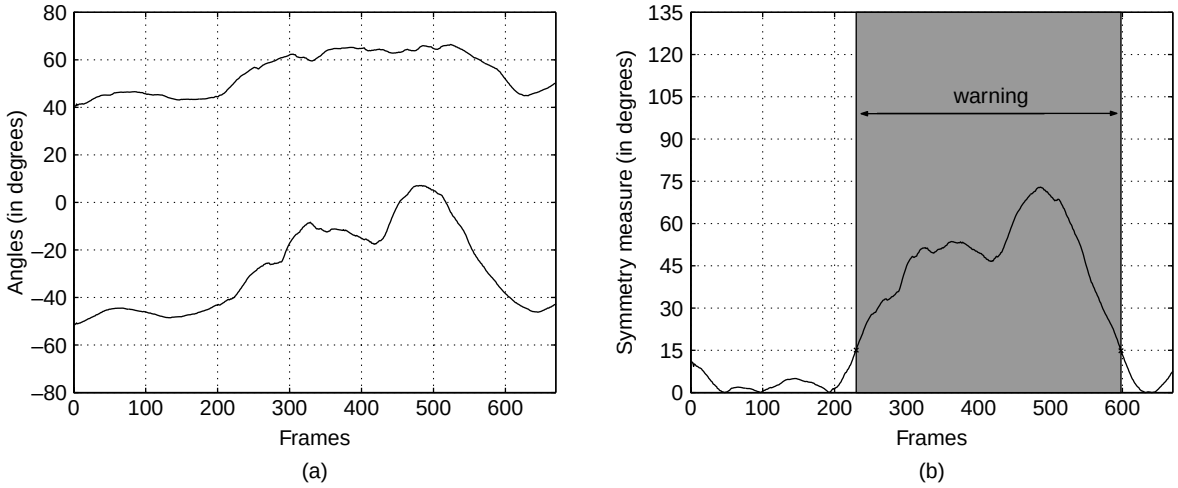

Fig. 12. (a) Orientations θ_r and θ_l for the second video sequence. (b) Corresponding symmetry measure α.

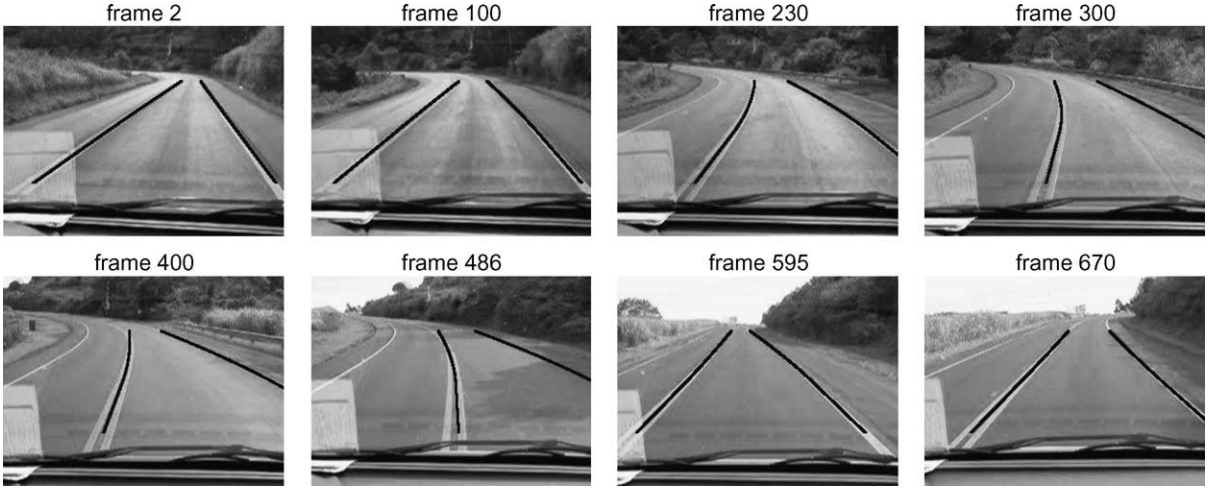

Fig. 13. Eight frames extracted from the second video sequence.

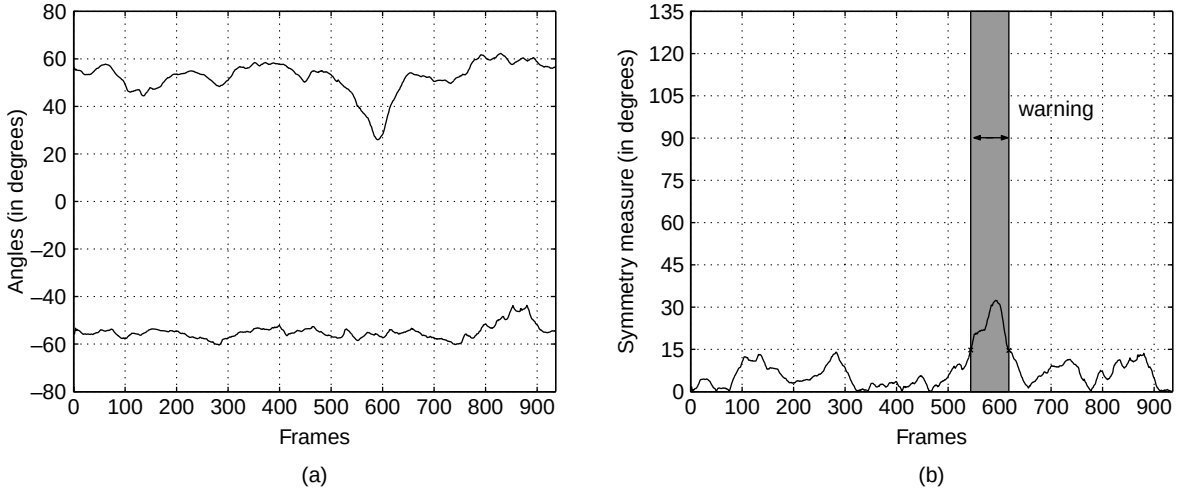

Fig. 14. (a) Orientations θ_r and θ_l for the third video sequence. (b) Corresponding symmetry measure α.

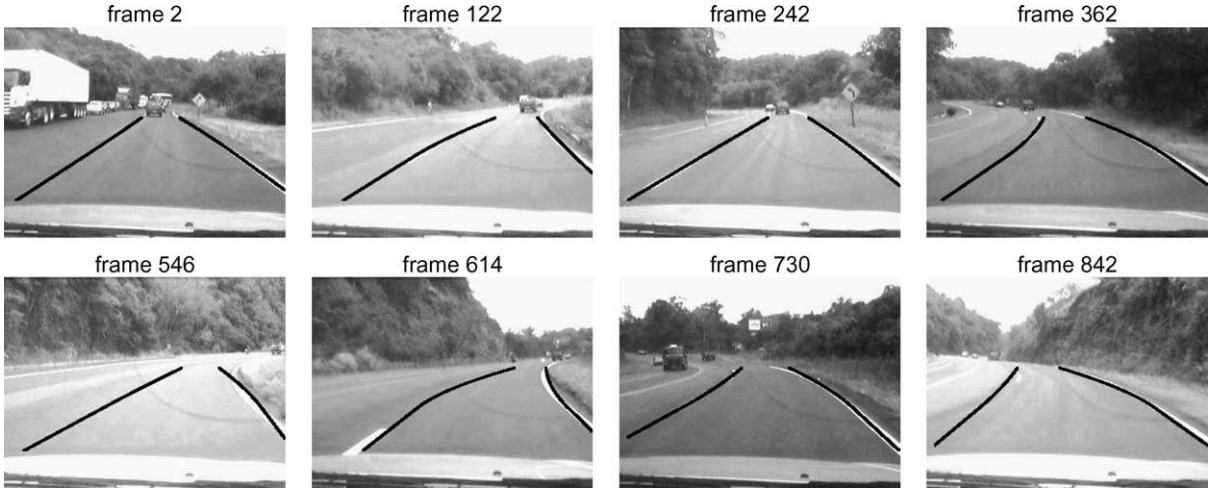

Fig. 15. Eight frames from the third video sequence.

An example of unwanted lane departure is depicted in Figs. 12 and 13, and concerns a video sequence containing 670 frames. Orientations θ_l and θ_r are shown in Fig. 12(a), and the corresponding symmetry measure β is illustrated in Fig. 12(b). A lane departure-warning signal was issued from frame 230 to frame 595 (such frames are marked with crosses in Fig. 12(b)). In fact, these frames are related to oversteering to the left on a curve, as shown in Fig. 13. Maximum deviation β occurred at frame 486, when the vehicle actually crossed lane boundaries. Our lane detection and following algorithm showed to be robust, despite the presence of several image artifacts in this video sequence (for example, shadows at frame 486, and varying texture and illumination conditions along frames).

Another video sequence was shot in a very curved road with several vehicles. Orientations and symmetry measure are illustrated in Fig. 14, and some frames of this video sequence are shown in Fig. 15. A false lane departure-warning signal was issued from frame 546 to 618, due to inaccurate estimation of orientation of the vehicle with respect to the right lane boundary. It can be noticed that there are drastic illumination changes (because there is a hill on the left of the road, that blocks the sun depending on the position of the vehicle). In particular, frame 546 is related to a right turn, and vegetation on the side of the road partially occludes lane markings. Furthermore, contrast between lane markings and vegetation is larger than contrast between lane markings and the road in frame 546. The combination of these factors causes an inaccurate fit of the proposed linear-parabolic model from frames 546–614, explaining the false alarm. In all other frames, the proposed model provides an accurate fit. Although our model also works in higher-curvature roads, we believe that lane departure warning systems are more useful in lower-curvature high-speed highways. First, driver sleepiness is more common in 'boring' straight or low-curvature roads; second, some drivers tend to 'cut' curves, which may produce several lane departure alarms.

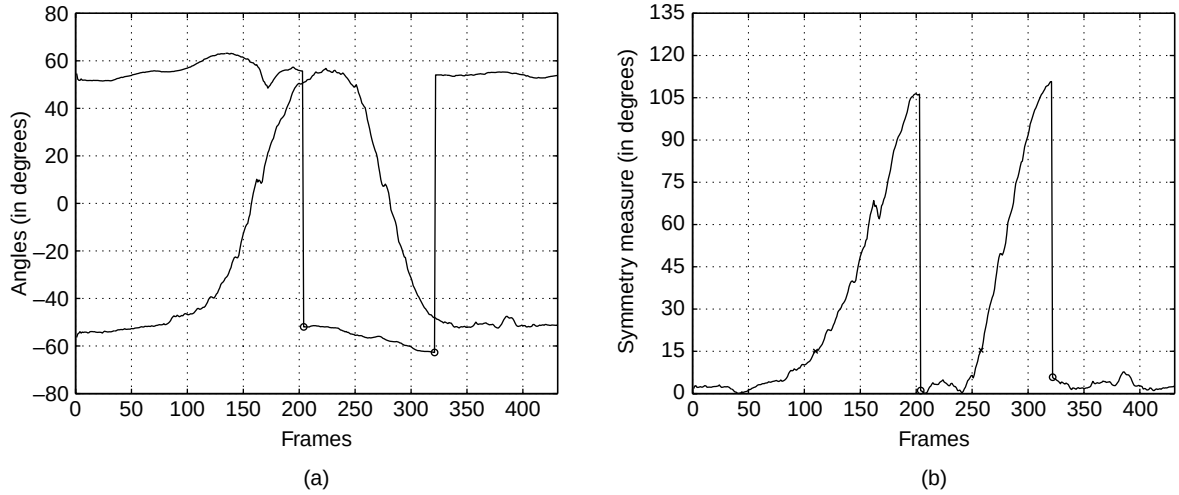

Fig. 16. (a) Orientations θ_r and θ_l for the fourth video sequence. (b) Corresponding symmetry measure α.

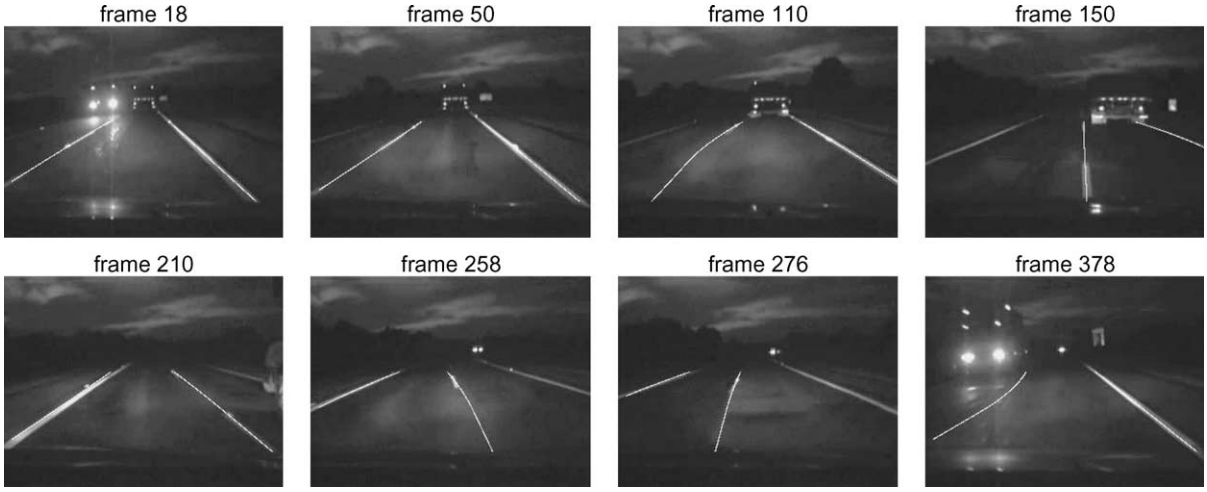

Fig. 17. Eight frames from the fourth video sequence.

We also tested the proposed technique for videos acquired at night. Orientations and symmetry measure for this sequence are illustrated in Fig. 16, and some frames are depicted in Fig. 17. A particular problem of nocturnal images is local image saturation caused by headlights of incoming vehicles, as shown in some frames of Fig. 17. Nevertheless, the linear-parabolic model provides a robust fit, and the lane departure systems detected a voluntary lane change (the vehicle was overtaking a truck).

5.1. Limitations

The main limitation of the proposed technique is regarded to significant occlusions of lane markings due to vehicles in front of the camera, as shown in Fig. 18(a). In fact, significant occlusions occur only when the vehicle in front is very close to the camera (less than 10 m), which typically happens only in traffic jam situations. Although the linear-parabolic model performs well in the presence of sparse shadows (such as irregular shadows cast by trees), it may present erroneous results if strong aligned shadows appear close to lane markings. In such cases, edges introduced by shadows may be stronger than edges related to lane markings, specially in dashed markings, as illustrated in Fig. 18(b).

Fig. 18. Limitations of the proposed technique. (a) Occlusion of lane markings. (b) Strong shadow causing an erroneous detection of lane boundaries.

6. Concluding remarks

In this paper, we proposed a new lane departure warning system based on a linear-parabolic lane boundary model. Initially, a combination of the EDF and the Hough transform is used to detect lane boundaries. Next, a linear-parabolic model is fit to lane boundaries in subsequent images by minimizing an energy measure. Finally, orientation of the vehicle with respect to both lane boundaries is computed, and a symmetry measure is used to detect unwanted lane changes in advance.

Our experimental results indicate that the proposed model provides an accurate fit to lane boundaries, and can be used to obtain robust information about their orientation. Also, these orientations are used to produce a symmetry measure, that correctly indicates tendencies of lane departure in advance (thus, providing enough time for the driver to correct his/her trajectory).

Further work will concentrate on extending the proposed model to estimate orientation of the vehicle with respect to both lane boundaries in world coordinates. This would enable active safety (the car could actually take over the steering wheel to prevent an accident) and autonomous driving.

Acknowledgements

The authors would like to thank Brazilian agency CNPq for financial support.

References

[1] J. Hagen, Road safety crisis, UN Chronicle Online Edition, http://www.un.org/Pubs/chronicle/2004/issue1/0104p78.asp
[2] Anuário Estatístico de Acidentes de Trânsito, Annual Report, DENATRAN, 2002, http://www.denatran.gov.br/acidentes.htm

[3] D.A. Pomerleau, RALPH: rapidly adapting lateral position handler, in: Proceedings of IEEE Intelligent Vehicles Symposium, Detroit, USA, 1995, pp. 506–511.
[4] M. Bertozzi, A. Broggi, GOLD: a parallel real-time stereo vision system for generic obstacle and lane detection, IEEE Transactions on Image Processing 7 (1) (1998) 62–81.
[5] W. Enkelmann, G. Struck, J. Geisler, ROMA: a system for model-based analysis of road markings, in: Proceedings of IEEE Intelligent Vehicles Symposium, Detroit, USA, 1995, pp. 356–360.
[6] Y. Wang, D. Shen, E. Teoh, Lane detection using catmull-rom spline, in: Proceedings of IEEE Intelligent Vehicles Symposium, Stuttgart, Germany, 1998, pp. 51–57.
[7] Y. Wang, D. Shen, E. Teoh, Lane detection using spline model, Pattern Recognition Letters 21 (6/7) (2000) 677–689.
[8] J. Park, J. Lee, K. Jhang, A. lane-curve, detection based on an LCF, Pattern Recognition Letters 24 (14) (2003) 2301–2313.
[9] Y. Wang, E. Teoh, D. Shen, Lane detection and tracking using B-snake, Image and Vision Computing 22 (4) (2004) 269–280.
[10] N. Apostoloff, A. Zelinsky, Robust based lane tracking using multiple cues and particle filtering, in: Proceedings of IEEE Intelligent Vehicles Symposium, Columbus, OH, 2003, pp. 558–563.
[11] J.C. McCall, M.M. Trivedi, An integrated, robust approach to lane marking detection and lane tracking, in: Proceedings of IEEE Intelligent Vehicles Symposium, Parma, Italy, 2004, pp. 533–537.
[12] D.J. LeBlanc, G.E. Johnson, P.J. Venhovens, G. Gerber, R.D. Sonia, R.D. Ervin, C.-F. Lin, A.G. Ulsoy, T.E. Pilutti, CAPC: a road-departure prevention system, IEEE Control Systems Magazine 16 (1996) 61–71.
[13] R. Risack, N. Mohler, W. Enkelmann, A video-based lane keeping assistant, in: Proceedings of IEEE Intelligent Vehicles Symposium, Dearborn, MI, 2000, pp. 506–511.
[14] J.W. Lee, A machine vision system for lane-departure detection, Computer Vision and Image Understanding 86 (1) (2002) 52–78.
[15] J.W. Lee, C.-D. Kee, U.K. Yi, A new approach for lane departure identification, in: Proceedings of IEEE Intelligent Vehicles Symposium, Columbus, OH, 2003, pp. 100–105.
[16] C.R. Jung, C.R. Kelber, A lane departure warning system based on a linear-parabolic lane model, in: Proceedings of IEEE Intelligent Vehicles Symposium, Parma, Italy, 2004, pp. 891–895.
[17] R. Duda, P. Hart, Use of the hough transform to detect lines and curves in pictures, Communications of the ACM 15 (1) (1972) 11–15.
[18] W.K. Pratt, Digital Image Processing, Wiley, New York, 1991.
[19] A. Rao, A Taxonomy for Texture Description and Identification, Springer, New York, NY, 1990.
[20] F. O'Gorman, M. Clowes, Finding picture edges through collinearity of feature points, IEEE Transactions on Computers 25 (4) (1976) 449–456.